Violin *f*-hole contribution to far-field radiation via patch near-field acoustical holography

George Bissinger
Physics Department, East Carolina University, Greenville, North Carolina 27858

Earl G. Williams and Nicolas Valdivia
Naval Research Laboratory, Washington, DC 20375

(Received 25 July 2006; revised 9 January 2007; accepted 1 March 2007)

The violin radiates either from dual ports (*f*-holes) or via surface motion of the corpus (top+ribs +back), with no clear delineation between these sources. Combining "patch" near-field acoustical holography over just the *f*-hole region of a violin with far-field radiativity measurements over a sphere, it was possible to separate *f*-hole from surface motion contributions to the total radiation of the corpus below 2.6 kHz. *A*0, the Helmholtz-like lowest cavity resonance, radiated essentially entirely through the *f*-holes as expected while *A*1, the first longitudinal cavity mode with a node at the *f*-holes, had no significant *f*-hole radiation. The observed *A*1 radiation comes from an indirect radiation mechanism, induced corpus motion approximately mirroring the cavity pressure profile seen for violinlike bowed string instruments across a wide range of sizes. The first estimates of the fraction of radiation from the *f*-holes F_f indicate that some low frequency corpus modes thought to radiate only via surface motion (notably the first corpus bending modes) had significant radiation through the *f*-holes, in agreement with net volume changes estimated from experimental modal analysis. F_f generally trended lower with increasing frequency, following corpus mobility decreases. The *f*-hole directivity (top/back radiativity ratio) was generally higher than whole-violin directivity. [DOI: 10.1121/1.2722238]

PACS number(s): 43.75.De, 43.40.At [JGM] Pages: 3899–3906

I. INTRODUCTION

General radiation properties of the violin have been measured since at least 1937 when Meinel[1] compared the radiation from a violin with and without a soundpost. In 1972 Meyer looked at the directivity patterns of violins, violas, cellos, and contrabasses, observing in the violin, for example, an evolution from nearly omnidirectional at low frequencies ($\lambda \geq$ size), few-lobed up to about 2 kHz and many-lobed above that.[2] All of these measurements, however, looked at the total radiation of the violin because there was no way to separate the dual port contribution (*f*-holes) from the surface motion radiation, the only two radiation sources for a violinlike instrument. Recently Wang and Burroughs,[3] using four measurement planes and planar near-field acoustical holography[4] (NAH), determined magnitudes and phases of volume flows from surface and port regions to give a more detailed view of radiation sources in the violin. (Driving force frequencies however were limited to open strings and harmonics up to 3 kHz only.) They observed that the area across the top plate in the C-bout (central) region around the bridge and soundpost (cf. their Fig. 3) was consistently a prominent region for radiation. However their spatial resolution at 294 Hz was not sufficiently good to demonstrate that radiation from *A*0, a Helmholtz-like cavity resonance near this frequency believed to radiate only through the *f*-holes, was indeed only from the *f*-holes and not partly from the corpus (top+ribs+back).

While various small substructures such as tailpiece, neck-fingerboard, bridge, and strings, were not important radiators, in agreement with general acoustic expectations,[5] much of acoustic importance about the compliant-wall violin corpus enclosing a dual-port cavity is still to be discovered. For example, corpus wall motions are capable of exciting various cavity modes, most prominently *A*0 (air modes all labeled with the prefix *A*), the lowest frequency strongly radiating mode in the violin or any other current bowed string instrument. Once any cavity mode is excited, and there are more than 40 cavity modes in the violin below 4 kHz,[6,7] the question of how strongly they in turn back-couple to the compliant corpus walls becomes important since pressure oscillations for modes below 1.3 kHz have already been observed to excite significant surface vibrations.

One such mode, *A*1, the first longitudinal cavity mode near 450 Hz coupled to *A*0,[8] has a nodal line crossing the *f*-hole region, suggesting an acoustic short; hence it should not radiate effectively through the *f*-holes, yet some violins have significant *A*1 radiation. Indeed for the violin octet a general trend of *A*1 radiation increasing with size relative to the nearby first corpus bending modes—the dominant low frequency corpus mode radiators in smaller instruments—actually led to it far outstripping radiation from these modes for the large bass.[9] If no radiation issued from the *f*-holes, but the violin overall still radiated, only an indirect radiation mechanism of cavity-mode-induced surface motion could be the cause.

Another interesting indirect radiation mechanism possibility is compliant wall motion associated with individual violin corpus modes resulting in substantial net cavity volume changes, which in turn are capable of forcing acoustically significant volume flows through the *f*-holes. At low

frequencies where $\lambda >$ violin size, and the air can be treated as approximately incompressible, experimental evidence can validate this mechanism.

These matters can only be resolved using advanced techniques with spatial resolution capable of unambiguously determining where the radiation originates. Such an experiment could ideally use NAH techniques since it is capable of determining surface and *f*-hole radiation equally well, but experimental difficulties in getting close to every part of the surface of the entire violin combined with the computational effort and measurement surface constraints for such an unusual shape make it impracticable at present. However a recent important variant of NAH, "patch" NAH (pNAH), where only a small part of a vibrating object is closely scanned and radiation from only the measured area, or some circumscribed portion thereof, is computed,[10,11] offers a practical alternative when combined with standard acoustical and vibrational measurements.[12]

Radiativity profiles, volume flows, relative phases, and radiation directivity for each *f*-hole, with special attention to the low frequency "signature" modes—$A0$ (Helmholtz-like cavity mode), $A1$ (first longitudinal cavity mode), CBR (‡ top and back plate nodal patterns), and $B1^-$ and $B1^+$ (first corpus bending modes)—were created from pNAH measurements. Computed volume flows through the *f*-holes were compared to estimated net volume flows from experimental modal analysis for selected normal modes below 0.8 kHz. Finally averaged-over-sphere far-field total radiativity combined with these pNAH computations for *f*-hole far-field radiation was used to provide the first estimates of the fraction of the violin's total far-field radiation emitted from the *f*-holes.

II. EXPERIMENTAL

A. Experimental modal and acoustic analysis

The experimental modal analysis and acoustic measurements as well as various analysis techniques have been extensively covered,[12] and so will not be covered here. A playable student violin (but without chinrest) chosen for its significant far-field averaged radiativity $\langle R \rangle$ (pressure/force, transfer function) for $A1$ near 450 Hz was employed to determine whether this cavity mode radiated directly through the *f*-holes or indirectly via induced wall motion. Excitation of the violin was always via an automated miniature force hammer striking the G-string corner of the violin bridge in the plane of the bridge parallel to the top plate surface similar to configuration shown in Fig. 1(a); pressure measurements were made over an $r=1.2$ m sphere in an anechoic chamber, with the violin supported "free-free" by two thin elastics, to compute top and back hemisphere $\langle R_{\text{top}} \rangle$ and $\langle R_{\text{back}} \rangle$ (the ratio $\langle R_{\text{top}} \rangle / \langle R_{\text{back}} \rangle$ defines the directivity $\langle D \rangle$) and, averaged-over-sphere $\langle R_{\text{total}} \rangle$ radiativities. These averaged radiativities are all comprised of *f*-hole and surface radiation contributions. The Fourier analysis was over 0–4 kHz, with $\Delta f=1.25$ Hz resolution, for the modal and acoustic measurements. A mobility profile of the violin top plate obtained with a scanning laser verified that mode frequencies, shapes, and mobility amplitudes had not changed significantly from an earlier complete scan over the entire violin.[13] Mobility data from the earlier scan were then used for the corpus. Another total radiativity $\langle R_{\text{total}} \rangle$ scan was performed to average with the earlier data. Radiativity errors incorporated ~5% support fixture losses that were neglected, ~5% microphone calibration errors, and ~3% excitation force angle/plane variations (all somewhat frequency dependent), for a combined nominal ±10% value.

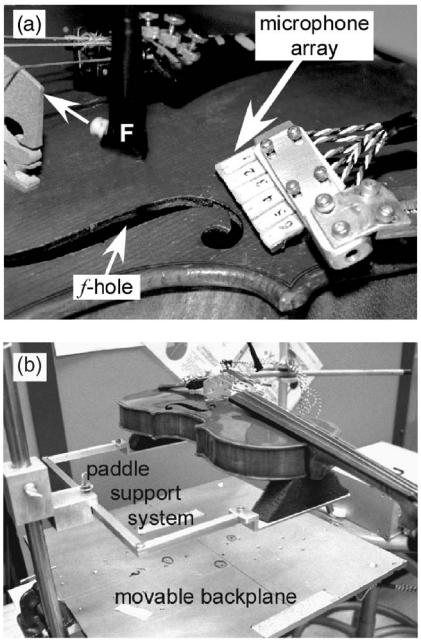

FIG. 1. (a) Translating-shifting microphone array over *f*-hole region with excitation force hammer at bridge corner driving point; (b) support paddle-variable backplane positioning setup with lab jack (not shown) under backplane.

B. "Patch" near-field acoustical holography

The pNAH measurements of *f*-hole radiation required very close, very accurate positioning of the scanning microphone array, a practical impossibility with the anechoic chamber support fixture and violin suspension where force hammer excitation created 2–3 mm low frequency residual rigid body motion. To eliminate the possibility of the microphone array striking and possibly scratching the surface an alternative suspension was necessary, placing the violin on two cut out foam pieces attached with double-sided tape to a rigid aluminum plate to support the end blocks. This arrangement had been used previously[14] and its effect on the violin's vibrational behavior was well understood: Raising rigid body mode frequencies to roughly 20 Hz, significantly higher than the thin elastic support system but still much lower than any corpus mode vibrational frequency (lowest ~400 Hz) so that any effect on mode frequencies and shapes would be small, and adding ~20% support fixture damping to the total, although all corpus mode dampings were still ≤1.2% of critical. Again these acoustic scans have nominal ±10% errors, after correction for the additional support fixture losses.

The pNAH microphone data were acquired over the same frequency range and Δf as the modal and acoustic data, using 6 Knowles EA-OKPL omnidirectional microphone

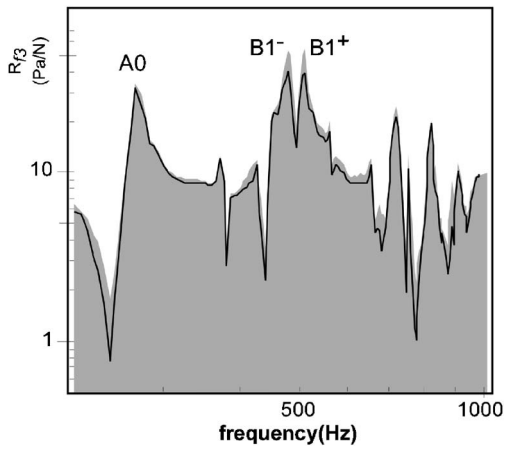

FIG. 2. Maximum (shaded) and minimum (thin line) radiativity R_{f3} for microphone 3 at mid-f-hole versus frequency over all backplane distances and absorber configurations. (Narrow structures are string resonances.) Especially note curve separation in $B1$ region.

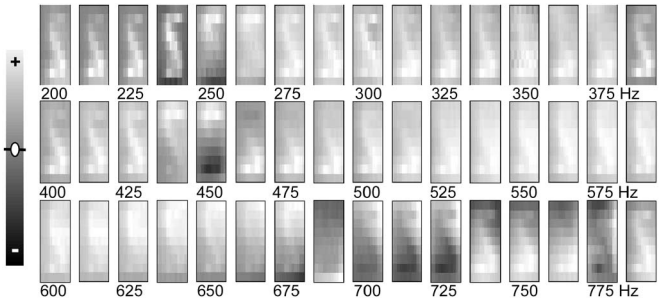

FIG. 3. A 12×9 array of raw radiativity data from bass bar side f-hole with scale denoting positive-negative values. Individual blocks correspond to 12.5 Hz interval stepped-frequency results (every tenth frequency step). Blurred f-hole outline clearly apparent.

modules mounted in a linear array oriented at ~45° to the scan plane as pictured in Fig. 1(a). The microphone spacing was 5.8 mm, but a calibrated shift of the array created an effective spacing of 2.9 mm. The array was translated using a specially constructed positioning support fixture to cover 9 steps with 1.05 cm spacing between each, starting just below, stepping along the length, and ending just above each f-hole, resulting in a 12×9 array of points for each f-hole. At each position of the array the excitation force on the violin was recorded simultaneously to create pNAH radiativity transfer functions so that relative acoustic phase information could be determined at each of the 108 points. The overall area covered by each plane was 26.8 cm^2, about 20% of which was taken up by the f-hole itself. The microphone array calibration was made using a white noise source in the anechoic chamber and an adjacent calibrated microphone.

Near-surface reflection/interference effects (herein labeled backplane loading) on measured pressures over the f-hole region were checked independently in another support fixture that placed the violin on the same foam supports now attached to a pair of thin support paddles that floated above the original $A1$ plate [Fig. 1(b)], which was placed on a lab jack to vary the violin-plate distance. Although this support fixture introduced some additional relative microphone-violin motion, pressure response variations could easily be observed as the backplane distance was varied. The microphone array was placed close to the bridge, with the innermost microphone at the bridge foot and the outermost microphone overlapping the edge of the violin.

A sequence of measurements, starting as close as possible to the original position ($1\times$) during actual measurements and then stepping to $2\times$, $4\times$, and $8\times$ the original distance (plus $8\times$ with Sonex© absorber foam), was used to observe systematic variations in microphone output. The output of microphone 3, directly over the middle of the f-hole, was used as a measure of backplane loading on radiation from the f-hole. Maximum and minimum radiativity values were extracted from this family of curves and plotted versus frequency in Fig. 2. Overall little significant backplane loading was observed across the 4 kHz range examined, with 8 $\times$ (with or without Sonex© foam) typically being the greatest, a few percent larger than $1\times$ results except in the minima. There was however one important exception: The first corpus bending modes near 500 Hz had a minimum radiativity at $1\times$ and maximum at $8\times$ for microphone 3, which corresponded to 19% and 29% changes, respectively. These values were used to correct for $B1^-$ and $B1^+$ backplane loading when computing the fraction of radiation from f-holes F_f.

With the foam support system on the rigid aluminum plate, it was possible to scan the array <1 mm from the irregular surface at the closest points without danger of violin motion creating accidental strikes on the microphone array. Over the entire scan the microphone-surface distance ranged from ~1 to ~4 mm. A 12×9 array of raw radiativity data from a complete scan over one f-hole is shown in Fig. 3.

C. "Patch" near-field acoustical holography

The raw radiativity data represent phased nearfield holograms that were processed to reconstruct the radiativity, normal velocity, and normal intensity in the plane of the f-hole.[10,11] Patch NAH provides accurate reconstructions and removes the need for holograms extending past the ends of the violin body, as was done by Wang and Burroughs.[3] The determination of the normal velocity in the f-hole plane provided by pNAH is difficult to measure by any other means and provides a direct measure of the volume flow from the f-holes. Furthermore, the determination of the normal acoustic intensity in the f-hole plane provides a means of computing the total power radiated from the f-hole alone.

NAH processing sharpens the raw microphone data (Fig. 3, showing blocks at every tenth frequency step, 12.5 Hz intervals) to give a much clearer outline of the f-hole in the final normal volume velocity display as shown in Fig. 4. The real part of the volume velocity is shown in Fig. 4, with positive and negative phase information provided by gray scale coding.

The NAH processing also provides detailed information on surface motion immediately adjacent to each f-hole that is directly comparable to mobility data gathered in a laser scan. Once the data have been NAH-processed, the final step is to demarcate the region from which radiation to the far field will be computed.

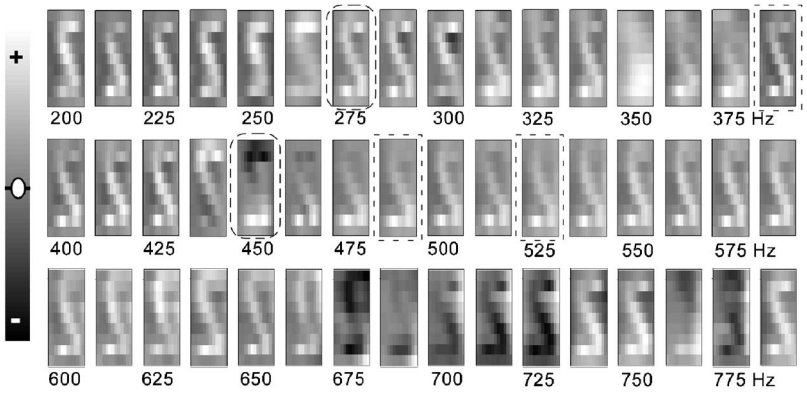

FIG. 4. Volume velocity derived from patch NAH using raw radiativity holograms (Fig. 3). The *f*-hole outlines are sharpened due to difference between motion of wood surrounding *f*-holes and the enclosed air. [Signature cavity $A0$ (~275 Hz) and $A1$ (~450 Hz), and corpus CBR (~387 Hz) and $B1^-$, $B1^+$ (~487 and ~525 Hz, respectively) modes are shown boxed.)

D. Boundary element model computations

To compute the radiation on an $r=1.2$ m sphere from the measured volume flow in the *f*-holes, a boundary element model employing a rigid violin-shaped corpus with *f*-holes was generated. BEM discretization decomposed the violin surface into 1326 linear triangular elements with 665 node points. Close to each *f*-hole, a special distribution of points corresponding to the NAH reconstructed velocity from the 12 by 9 array of microphone points was inserted. Figure 5 shows the element distribution of the violin surface with the increased density of elements near and in the *f*-hole regions. This boundary element decomposition of the violin surface was used to create a matrix transfer function via the direct-explicit approach[15] to take velocity into acoustical pressure over the surface of the sphere. In the Results section the measured radiativity from the *f*-holes alone as determined from pNAH and the BEM projection is compared with the direct measurement of the violin total radiativity in an anechoic chamber.

III. RESULTS

The pNAH radiativity data from the *f*-hole scans were used to extract: (1) surface and volume velocities over the scanned area, (2) comparisons of $A0$ radiation with Cremer model monopole predictions in the top hemisphere,[16] (3) radiation patterns for far-field pressures from the *f*-holes only (using the BEM model), at selected frequencies for a few important individual modes, (4) an averaged-over-sphere far-field radiativity $\langle R_f \rangle$ at 1.2 m from measured *f*-hole volume velocities (and the BEM model) for comparison with $\langle R_{\text{total}} \rangle$ measured in the anechoic chamber to compute fraction of acoustic energy radiated from both *f*-holes F_f, and (5) the directivity $\langle D_f \rangle$ of radiation from the *f*-holes (computed from the ratio of averaged top to back plate hemisphere radiativities) for comparison with equivalent directivity $\langle D \rangle$ computed from the anechoic chamber total radiativity measurements. All of these are new results for the violin.

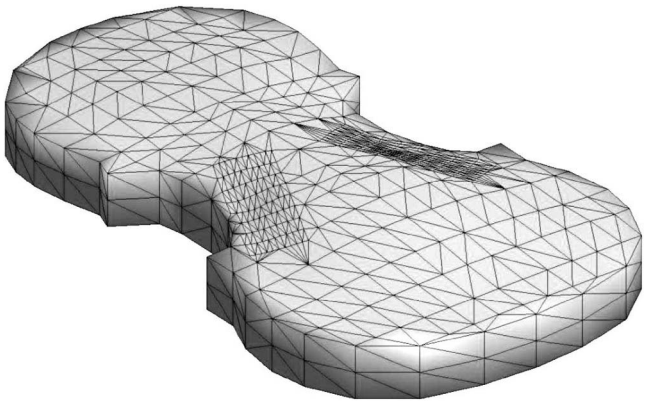

FIG. 5. BEM geometry model to compute far-field radiativity using pNAH *f*-hole volume velocity profiles. Note insertion of *f*-hole measurement grids over violin corpus grid.

A. Surface and volume velocities

All of the low frequency cavity and corpus modes of the violin up to about 600 Hz (sometimes called signature modes) are readily identifiable from violin to violin, and will be discussed individually due to their importance for the sound in the open-string pitch region. Above this range variations in individual materials and construction methods modify mode shapes and so interviolin mode comparisons become unreliable and statistical measures become necessary. Fortunately above 1 kHz the violin also enters a frequency region where (a) the radiation efficiency has increased so that all modes radiate well and (b) significant mode overlap is common. Hence the importance of individual modes decreases, justifying the statistical approach.

Referring to the results shown in Fig. 4 for $A0$ near 275 Hz and $A1$ near 453 Hz, there is essentially zero surface motion for both modes (midgray outside *f*-holes) compared with the volume velocity in the *f*-holes. $A1$ however induces significant cavity wall motions in the upper and lower bout regions of the violin that reflect the pressure polarity reversal of this first longitudinal cavity mode, leading to a surface motion nodal area in the central *C*-bout region. $A0$ has all positive volume velocities over the *f*-holes as expected, while $A1$ shows a polarity reversal corresponding to its expected node at the *f*-hole, producing an intra-*f*-hole acoustic short that signifies weak far-field radiation from the *f*-holes.

A further demonstration of the detail available from these NAH scans comes from expanding the display to include both *f*-holes for two signature modes in Fig. 6. The CBR mode looks like a rhomboid in the *C*-bout region cross-section, with ‡ top and back plate nodal patterns that indicate weak radiation from the corpus of the violin. Note that the CBR mode *f*-hole air motion on both sides of the violin is out of phase with the top plate motion immediately adjacent

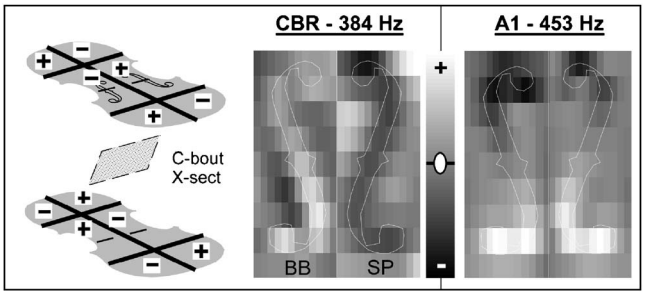

FIG. 6. Acoustic shorts (*f*-hole outlines superimposed): *inter-f*-hole for the CBR mode (plate nodal lines and *C*-bout cross section shown); *intra-f*-hole for *A*1. (Bass bar–soundpost sides notated in CBR.)

to it, indicating an inter-*f*-hole acoustic short for the *f*-hole radiation. The CBR mode is a good example of a mode with approximately zero radiation damping, hence its total damping consists of just internal damping.

Finally, no example of negligible air motion in the *f*-holes was observed below 2.5 kHz in the pNAH results, irrespective of the motion or lack of motion of the surface immediately adjacent to the *f*-holes, or its in- or out-of-phase behavior relative to the *f*-holes. This observation underscores the highly vibroacoustic character of the violin's dynamic response where the mechanical motions of the corpus affect the enclosed air motions, while enclosed air oscillations affect corpus motions.

B. *A*0 monopole radiativity

The *f*-hole monopole radiation of *A*0 was computed directly from Cremer's lumped element mode,[16] which assumes that the excitation force on the bridge drives a plate stiffness (spring) in series with a parallel branch consisting of the air cavity stiffness in parallel with the air-slug mass in the *f*-holes (Cremer's equations 10.11a and 10.14). In addition a resistance due to air viscosity was assumed in series with the air-slug mass to limit the *f*-hole resonance to a finite radiated pressure. Once the volume flow q_0 in the *f*-hole is determined, the radiated pressure p_f at $r=1.2$ m is determined using the simple monopole formula, $p_f = -i\omega\rho q_0(e^{ikr}/4\pi r)$. In this model it was assumed that the total Q (viscous+radiation damping) was 20 (from anechoic chamber measurement results), and that the vibrating plate area (S_1 in Cremer's model) was 500 cm^2. It is remarkable how closely Cremer's model prediction compares with the direct measurement of radiativity $\langle R_{\text{top}}\rangle$ (see Fig. 7).

To compute the radiated pressure (always normalized to 1 N force) on a sphere of radius 1.2 m from the pNAH measurements the normal velocity reconstructed in each *f*-hole (Fig. 4 shows bass-bar side *f*-hole results) was inserted into the BEM model. The normal velocities at all BEM nodes except the nodes in each *f*-hole were set to zero. Thus the violin body acts as a rigid baffle, with radiation only from the *f*-holes. The pressure was spatially averaged over the violin top and back hemispheres individually or combined, to produce pNAH averages analogous to those computed for the experimental radiativities (Sec. II A). A measure of *f*-hole radiation directivity $\langle D_f\rangle$ was computed from ratio of pNAH top-to-back pressures, again analogous to the experimental estimates. (Radiativity units are always Pa/N indicating normalization to driving force on bridge.) The pNAH predictions of *A*0 radiation from the *f*-holes into the top hemisphere are compared in Fig. 7 with the Cremer monopole and $\langle R_{\text{top}}\rangle$ results. The agreement within experimental error with the direct measurement at the *f*-hole resonance frequency of ~275 Hz indicates that the *A*0 radiation is due solely to the volume flow out of the *f*-hole, confirming prior assumptions about this mode.

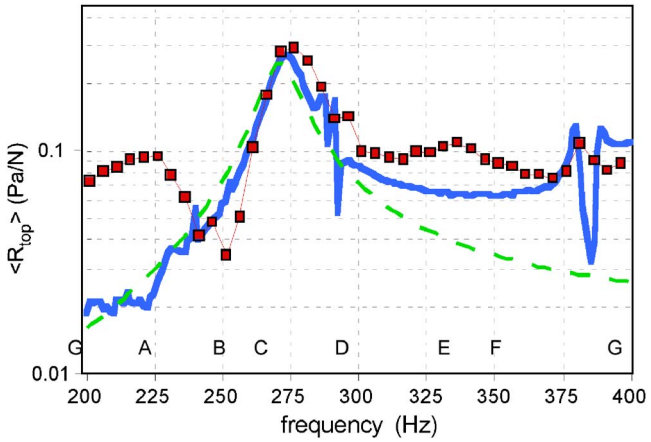

FIG. 7. (Color online) Comparison among monopole model for Helmholtz resonance *A*0 ($Q=20$, $S_1=500$ cm^2; dashed line), pNAH prediction (-■-), and measured (solid line) top hemisphere total radiativities. (Approximate violin fingered pitches starting at open *G* shown for reference.)

Note that below this resonance from 200–230 Hz the averaged top hemisphere *f*-hole radiativity was considerably larger than the violin $\langle R_{\text{top}}\rangle$. The explanation is simple (as hinted in Fig. 4) the corpus near the *f*-hole vibrates 180° out of phase with the air velocity in the *f*-hole. This 180° phase change results in a volume flow cancellation dramatically reducing the radiation from the complete violin. Mathematically, resorting again to Cremer's model (ignoring losses for simplicity) we can rewrite it as $q_0 = -[1/1-(\omega/\omega_H)^2]q_b$, where q_b is the total outward volume flow of the corpus and ω_H is the *f*-hole resonance frequency. This equation demonstrates the fact that as $\omega \to 0$, $q_0 \to -q_b$ and the volume flow from the *f*-holes is equal, and opposite, to the volume flow from the corpus. Above the *f*-hole resonance the volume flows from the corpus and *f*-holes would tend to be in phase, according to the above equation. However, Cremer's model fails to incorporate the presence of higher corpus modes and relative phase with these, a point addressed by Schelleng,[17] or to incorporate the coupling between *A*0 and the next higher (first longitudinal) cavity mode *A*1.[8] Clearly the various phase cancellations and couplings must be incorporated properly before such matters can be discussed appropriately.

C. *f*-hole radiation patterns for low frequency modes

The far-field *f*-hole radiation pattern for *A*0 is approximately isotropic at 1.2 m as can be seen from Fig. 8, with $\langle D_f\rangle = 1.08$. This is quite similar to the value of 1.15 for the overall violin directivity $\langle D\rangle$, computed from the anechoic chamber measurement ratio $\langle R_{\text{top}}\rangle/\langle R_{\text{back}}\rangle$. The radiation pat-

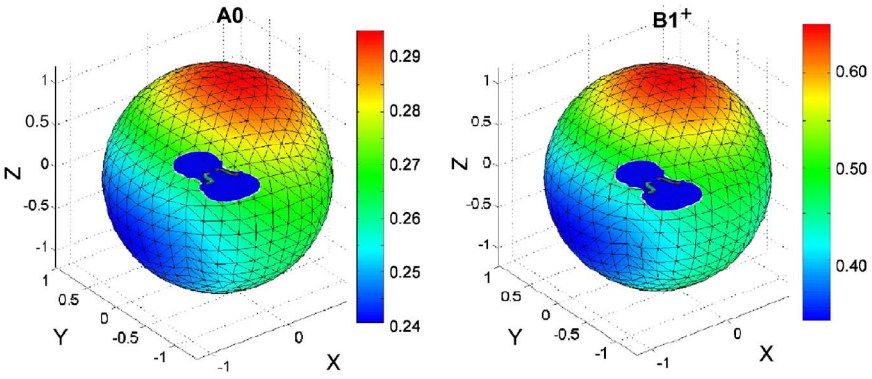

FIG. 8. (Color online) Computed pNAH *f*-hole radiation patterns (Pa/N) shown as color plots on a sphere with $r=1.2$ m for (1) *A*0 at 270 Hz and (r) $B1^+$ at 521 Hz. $B1^-$, the lower first corpus bending mode, has a shape very similar to $B1^+$. (Violin top plate in overlay for orientation.)

tern was computed using BEM for a motionless corpus (baffle) as described above and the pNAH results for the *f*-hole volume flow. This result is unsurprising since *A*0 has a wavelength ($\lambda \approx 1.25$ m) much greater than any *f*-hole or plate dimension. The *f*-hole radiation pattern for the $B1^-$ and $B1^+$ modes is also close to isotropic with $\langle D_f \rangle = 1.23$ and 1.27, close to the overall violin $\langle D \rangle = 1.01$ and 1.31, respectively. Neither *A*1 nor CBR modes radiated significantly through the *f*-holes (see Fig. 6).

D. Total versus *f*-hole radiativity

With the *f*-hole volume velocity it is straightforward to compute a pNAH radiativity into the top hemisphere for comparison to the analogous averaged farfield top radiativity $\langle R_{\text{top}} \rangle$ measured in the anechoic chamber.[13] The comparison is presented in Fig. 9. As expected, within our total and pNAH radiativity errors, *A*0 radiates entirely from the *f*-holes. On the other hand, the dip at *A*1 indicates no significant radiation through the *f*-holes, confirming the long-held belief that since these fall near a node for *A*1 (created of course by the *f*-holes themselves) there would be an acoustic

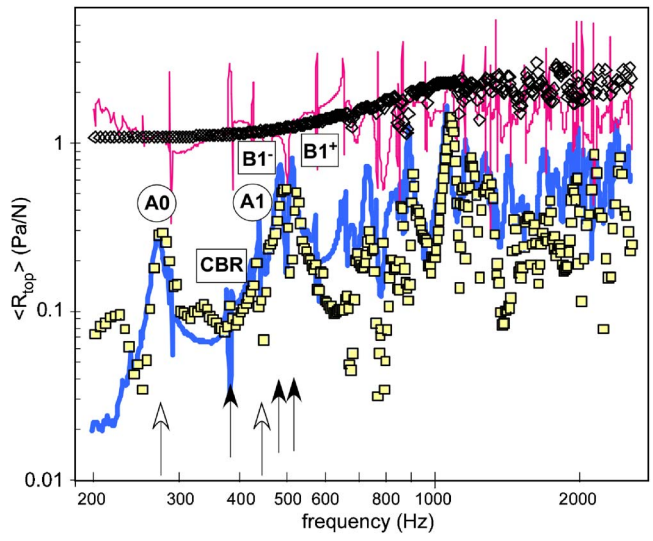

FIG. 9. (Color online) Lower curves: Top hemisphere pNAH radiativity from *f*-holes (□) versus $\langle R_{\text{top}} \rangle$ (thick line) up to 2.6 kHz. (Narrow structures due to undamped string resonances.) Upper curves: *f*-hole directivity $\langle D_f \rangle$ (◇) versus violin directivity $\langle D \rangle$ (thin line). (Signature cavity modes noted with open arrows and corpus modes with filled arrows.)

short in the *f*-holes. Consequently the sole source of the measured total radiativity must be the *A*1-induced surface vibrations.

As can be seen from Fig. 9 *A*1 is not a major radiating mode for this violin. Even though Schelleng completely dismissed *A*1 and higher cavity modes as significant radiators in his original violin octet scaling, *A*1 has been observed to evolve in strength to finally become *the* major radiator in the "main wood" region for the large bass member of the violin octet.[18] The source of the large bass' radiation in this region, assuming insignificant *A*1 radiation through the *f*-holes as observed in this violin experiment, must therefore come primarily from induced surface motion.

Another new result from Fig. 9 is that some corpus modes radiate strongly through the *f*-holes. For example, a major part of this violin's first corpus bending modes' overall radiation is *indirect* through the *f*-holes, not direct from surface motion. For certain "corpus" modes the fraction of the radiation from the *f*-holes approaches 1, e.g., the corpus mode near 1.1 kHz. This surprising result further complicates our understanding of violin sound because it concerns a hitherto unexamined source of radiation.

A brief summary of the significant direct and indirect violin radiation mechanisms discovered to date seems in order here: *Cavity* modes radiating (1) directly through the *f*-holes such as *A*0, or (2) indirectly through induced cavity wall vibrations such as *A*1 (and *A*2 and possibly higher cavity modes in larger instruments[18]); corpus modes radiating (3) directly from the surface (most modes) and/or (4) indirectly through the *f*-holes.

E. Mechanical estimate of volume flow

The experimental modal analysis (EMA) results provide an independent albeit crude check on this indirect corpus mode radiation path since the mobility scans covered almost the complete violin corpus. By scaling the normal mode mobility results in the modal analysis program to compliance (displacement/force) and using surface areas for each corpus substructure in the violin it was straightforward to make a rough mechanical estimate of volume changes over a cycle for individual normal modes. Approximate estimates of the volume flow out of the *f*-holes are possible if the air inside can be considered incompressible, restricting computations to modes that have $\lambda >$ violin length ($f < 800$ Hz). An additional caution—the pNAH computations were done at a par-

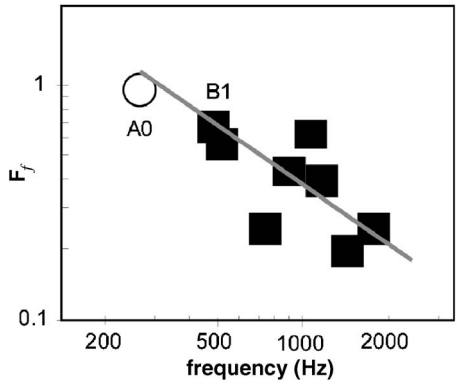

FIG. 10. Fraction of total radiation from *f*-holes F_f for normal modes below 2 kHz [symbol: (○) A_0, (■) corpus modes, and nominal errors ≈ symbol size]. Trendline (corpus modes only) to guide eye.

ticular frequency and thus incorporate whatever normal modes were participating at whatever level and relative phase in the overall vibration at this frequency (some indication of overlap can be seen in Fig. 9), whereas our normal mode volume changes were computed for one particular mode only, with no participation from other modes. Hence some variation between EMA and pNAH results must be expected, especially for overlapping modes, although at the peak of an isolated strong mode it is a good assumption that this mode dominates the measured overall mobility.

The EMA *f*-hole volume flow calculations were performed for $A0$, the first corpus bending modes $B1^-$ and $B1^+$ and a strong mode near 730 Hz (Fig. 9). Because $A0$ is not a corpus mode—although some corpus motion obviously is required to excite $A0$—its corpus volume change should be much less than its volume flow would imply; the estimated EMA volume flows for $A0$ were 323 $cm^3/s/N$, much less than the 2290 $cm^3/s/N$ pNAH estimates. The corpus mode EMA versus pNAH *f*-hole volume flow comparisons for $B1^-$ were 1571 versus 2343 $cm^3/s/N$, for $B1^+$ 2689 versus 2088 $cm^3/s/N$, and 1695 vs 755 $cm^3/s/N$ for the mode at 735 Hz. $A0$ corpus motion-induced volume flow estimates were only 14% of the pNAH value, the lowest ratio by far and too weak to result in the observed average radiativity at 1.2 m. The corpus modes had much larger EMA/pNAH volume flow ratios, ranging from 0.67 to 2.24, considered nominally equivalent for these crude estimates. It is worth noting that Saunders, using a bowing machine for excitation and a silk fiber observed through a microscope, saw some indication of *f*-hole air motion for the violin "main body" resonance (now $B1^- - B1^+$) but no higher body modes.[19]

F. Fraction of radiation from *f*-holes

Using separate averaged-over-a-sphere *f*-hole $\langle R_f \rangle$ and total radiativity $\langle R_{\text{total}} \rangle$ results, estimates of the fraction of violin radiation from the *f*-holes $F_f = \langle R_f \rangle / \langle R_{\text{total}} \rangle$ were computed for strongly excited modes up to 2.6 kHz (first corpus bending modes corrected for backplane air loading); above this frequency pNAH calculations were not carried out. These results are shown in Fig. 10 along with a superimposed trendline. The overall falloff in F_f results from the fusion of two dynamic trends: Less corpus motion (typically corpus mobility falls off at frequencies $> \sim 1$ kHz) and increased radiation efficiency (up to critical frequency ~4 kHz for violins,[20] where the radiation efficiency plateaus) as frequency increases. Thus steadily decreasing surface motion, which implies smaller volume flows, combined with steadily increasing ability to turn surface motion into radiation leads to the general conclusion that the fraction of acoustic energy radiated through the violin *f*-holes will diminish steadily with increasing frequency, even above the critical frequency; extrapolating from the trendline F_f drops to ~0.1 at 4 kHz. Interestingly, much of the radiation from a guitar in the lower octaves—in addition to the cavity resonance radiation—was also observed to issue from the sound hole in the earliest application of NAH to a musical instrument,[21] and back plate motions were often the major reason for the volume flow, rather than the top plate (confirmed by later modal analysis of another acoustic guitar[22]).

An interesting general argument to support "breathing" behavior of a violin based on conservation of momentum principles was provided by Cremer based on a simplistic 4-mass model of the violin,[23] where the center of mass of the violin must remain fixed, hence the top and back plates, which comprise most of the violin's mass, must vibrate in opposite phases, creating an overall breathing behavior to provide most of the radiation at low and possibly midfrequencies. Cremer also noted that the nonzero mass and kinetic energy of the ribs in this 4-mass model led to two "chief body resonances," not one, possibly analogs to the two first corpus bending modes, $B1^-$ and $B1^+$. However an earlier experiment examining removal of the violin soundpost on a violin's mode frequencies and shapes indicates that one of the first corpus bending modes disappeared.[24]

G. Directivity

The anechoic chamber measurements were used to compute a simple measure of radiation directivity $\langle D \rangle$ from a ratio of top to back averaged-hemisphere radiativities as presented in Fig. 9. Although $\langle D \rangle$, which includes the corpus and *f*-hole contributions, showed structure as different violin modes were traversed a gradual general rise from ~1 at the lowest frequencies, where $\lambda >$ violin size and hence nominally isotropic radiation is expected, to ~2 at 4 kHz was observed for all violins.[13] The *f*-hole directivity $\langle D_f \rangle$ showed little structure below 1 kHz, but considerably more above. $\langle D_f \rangle$ rises more rapidly than $\langle D \rangle$, but appears to roughly plateau above 1.2 kHz. This behavior appears to be of some value to violinists at low frequencies, always the least efficient region, when the violin is held as usual, canted at an angle toward the audience. Since radiation from the top would be more effective in reaching the audience, the *f*-hole contribution—raising the overall directivity at lower frequencies—somewhat enhances the effective ability to radiate toward the audience.

IV. CONCLUSIONS

Details inherently accessible in a fine mesh patch NAH experiment have greatly increased our ability to understand

some of the complexities of violin *f*-hole radiation. These first pNAH measurements on a musical instrument have given us important insights into *intra-* and *inter-f*-hole phase relationships, volume flow phase relationships with immediately adjacent surface motions, radiation from only the *f*-holes of the violin, and the basic direct and indirect radiation mechanisms of the violin. When used in combination with standard acoustic far-field measurements we find that the *f*-holes participate in the overall radiation from the violin far more than previously supposed, with many low frequency "corpus" modes radiating strongly, even predominantly, through the *f*-holes.

To some extent the already complex problem of understanding how the violin radiates has been complicated further, even though evidence for vibroacoustic coupling has been around a long time. The two traditional violin direct radiation mechanisms—*A*0 cavity mode radiation from the *f*-holes and corpus modes radiating from the surface—have now been joined by two indirect mechanisms—cavity-mode-induced wall vibrations and corpus-motion-induced air flow through the *f*-holes. Because *A*0 and *A*1 have been observed to dominate radiation in the open string region for some very large bowed string instruments, while indirect radiation through the *f*-holes modes can dominate the total radiation for some low frequency major corpus radiators in smaller instruments, it has become clear that all four of these radiation mechanisms must be accounted for in any complete analysis of the radiation from violins and other members of the bowed string instrument family.

ACKNOWLEDGMENTS

We would like to acknowledge the assistance of Janice Debro in acquisition of the pNAH data, and Knowles Acoustics for providing the miniature microphones. This research, performed as part of the VIOCADEAS Project, was supported by the National Science Foundation (DMR-9802656; GB) and by the Office of Naval Research (EGW and NV).

[1]H. Meinel, "On the frequency curves of violins," Akust. Z. **2**, 22–33 (1937).
[2]J. Meyer, "Directivity of string instruments," J. Acoust. Soc. Am. **51**, 1994–2009 (1972).
[3]L. M. Wang and C. B. Burroughs, "Acoustic radiation from bowed violins," J. Acoust. Soc. Am. **110**, 543–555 (2001).
[4]E. G. Williams, *Fourier Acoustics: Sound Radiation and Nearfield Acoustical Holography* (Academic, London, UK, 1999).
[5]G. Bissinger and A. Gregorian, "Relating normal mode properties of violins to overall quality: part I: signature modes," Catgut Acoust. Soc. J. **4**, 37–45 (2003).
[6]E. Jansson, "On higher air modes in the violin," Catgut Acoust. Soc. Newsletter **19**, 13–15 (1973); "Acoustical properties of complex cavities. Prediction and measurements of resonance properties of violin-shaped and guitar-shaped cavities," Acustica **37**, 211–221 (1977).
[7]G. Bissinger, "Acoustic normal modes below 4 kHz for a rigid, closed violin-shaped cavity," J. Acoust. Soc. Am. **100**, 1835–1840 (1996).
[8]G. Bissinger, "A0 and A1 coupling, arching, rib height, and *f*-hole geometry dependence in the 2-degree-of-freedom network model of violin cavity modes," J. Acoust. Soc. Am. **104**, 3608–3615 (1998).
[9]G. Bissinger, "Modal analysis of a violin octet," J. Acoust. Soc. Am. **113**, 2105–2113 (2003).
[10]E. G. Williams, "Continuation of acoustic near-fields," J. Acoust. Soc. Am. **113**, 1273–1281 (2003).
[11]E. G. Williams, B. H. Houston, and P. C. Herdic, "Fast Fourier transform and singular value decomposition formulations for patch nearfield acoustical holography," J. Acoust. Soc. Am. **114**, 1322–1333 (2003).
[12]G. Bissinger, "A unified materials-normal mode approach to violin acoustics," Acustica **91**, 214–228 (2005), and references therein.
[13]G. Bissinger and J. C. Keiffer, "Radiation damping, efficiency, and directivity for violin normal modes below 4 kHz," Acoust. Res. Lett. Online **4**, 7–12 (2003). http://scitation.aip.org/ARLO.
[14]K. Ye and G. Bissinger, "Attaining 'free-free' normal mode frequency *and* damping conditions for the violin," *Proc. 18th Intern. Modal Analysis Conf.- Soc. Exp. Mechanics*, Bethel, CT, 2000, pp. 398–403.
[15]N. Valdivia and E. G. Williams, "Implicit methods for NAH," J. Acoust. Soc. Am. **116**, 1559–1572 (2004).
[16]L. Cremer, *The Physics of the Violin, translated by J. Allen* (MIT Press, Cambridge, MA, 1983), Chap. 10.
[17]J. Schelleng, "On polarity of resonance," Catgut Acoust. Soc. Newslett. **10**, 14–21 (1968).
[18]G. Bissinger, "Modal analysis of a violin octet," J. Acoust. Soc. Am. **113**, 2105–2113 (2003).
[19]F. A. Saunders, "Recent work on violins," J. Acoust. Soc. Am. **25**, 491–498 (1953).
[20]G. Bissinger, "The role of radiation damping in violin sound," Acoust. Res. Lett. Online **5**, 82–87 (2004). http://scitation.aip.org/ARLO.
[21]W. Strong, T. B. Beyer, D. J. Bowen, E. G. Williams, and J. D. Maynard, "Studying a guitar's radiation properties with nearfield holography," J. Guitar Acoust. **6**, 50–59 (1982).
[22]C. D. Van Karsen and R. Sun, "Experimental modal analysis and operating deflection shapes of an acoustic guitar," *Proc. 15th Intern. Modal Analysis Conf.– Soc. Exp. Mechanics*, Bethel, CT, 1997, pp. 686–691.
[23]L. Cremer, "Remarks on the predictions of eigenmodes of violins," Catgut Acoust. Soc. J. **1**, 1–5 (1990).
[24]G. Bissinger, "Some mechanical and acoustical consequences of the violin soundpost," J. Acoust. Soc. Am. **97**, 3154–3164 (1995).